

Journal: Physical Review Applied

Accession code: LC19350N

Article Title: Practical Range Sensing with Thermal Light

First Author: Peng Kian Tan

AUTHOR QUERIES - TO BE ANSWERED BY THE CORRESPONDING AUTHOR

The following queries have arisen during the typesetting of your manuscript. Please answer these queries by marking the required corrections at the appropriate point in the text.

Q1	Please note that spacing, hyphenation, and formatting have been standardized throughout to comply with journal style. Also, minor copyediting changes have been made throughout the paper to follow journal and grammar guidelines and to allow improved readability. Please check the redlined proof to ensure that your meaning has not been changed.
Q2	Please carefully check all formulas, display equations, spacing, punctuation, font style (such as italic, roman, and bold), accents, and special characters throughout, including in the Abstract and endnotes.
Q3	Please check the order and appearance for all parts of all figures. Also note that the figure labels have been adjusted so that the roman and italic characters match the main text. Please check and confirm that no errors have been introduced.
Q4	As per journal style, claims of novelty and priority are not allowed. The sentences “A relevant...” and “Another useful property...” have been reworded to avoid the claim. See APS’s policy at http://journals.aps.org/authors/new-novel-policy-physical-review . Please check.
Q5	As per journal style, we have amended \approx to “approximately equal to”. Please check.
Q6	Please provide missing page number for Refs. [19, 24 and 25].

Important Notice to Authors

Attached is a PDF proof of your forthcoming article in Physical Review Applied. The article accession code is LC19350N. Your paper will be in the following section of the journal: RESEARCH ARTICLES

Please note that as part of the production process, APS converts all articles, regardless of their original source, into standardized XML that in turn is used to create the PDF and online versions of the article as well as to populate third-party systems such as Portico, Crossref, and Web of Science. We share our authors' high expectations for the fidelity of the conversion into XML and for the accuracy and appearance of the final, formatted PDF. This process works exceptionally well for the vast majority of articles; however, please check carefully all key elements of your PDF proof, particularly any equations or tables.

Figures submitted electronically as separate PostScript files containing color appear in color in the journal.

No further publication processing will occur until we receive your response to this proof.

ORCIDs

Please follow any ORCID links (DOI) after the authors' names and verify that they point to the appropriate record for each author. Requests to add ORCIDs should be sent no later than the first proof revisions. If authors do not subsequently add/authenticate ORCIDs within seven business days, production of the paper will proceed and no further requests to add ORCIDs will be processed. See complete details regarding ORCID requests and ORCID verification at <https://journals.aps.org/authors/adding-orcids-during-proof-corrections>.

NOTE: If this paper is an Erratum or a Reply, the corresponding author's ORCID may be present if previously provided to APS, but no ORCIDs can be added at proof stage.

Crossref Funder Registry ID:

Information about an article's funding sources is now submitted to Crossref to help you comply with current or future funding agency mandates. Crossref's Funder Registry (<https://www.crossref.org/services/funder-registry/>) is the definitive registry of funding agencies. Please ensure that your acknowledgments include all sources of funding for your article following any requirements of your funding sources. Where possible, please include grant and award ids. Please carefully check the following funder information we have already extracted from your article and ensure its accuracy and completeness:

- Quantum Engineering Programme

Other Items to Check

- Please note that the original manuscript has been converted to XML prior to the creation of the PDF proof, as described above. Please carefully check all key elements of the paper, particularly the equations and tabular data.
- Title: Please check; be mindful that the title may have been changed during the peer review process.
- Author list: Please make sure all authors are presented, in the appropriate order, and that all names are spelled correctly.
- Please make sure you have inserted a byline footnote containing the email address for the corresponding author, if desired. Please note that this is not inserted automatically by this journal.
- Affiliations: Please check to be sure the institution names are spelled correctly and attributed to the appropriate author(s).
- Receipt date: Please confirm accuracy.
- Acknowledgments: Please be sure to appropriately acknowledge all funding sources.
- Hyphenation: Please note hyphens may have been inserted in word pairs that function as adjectives when they occur before a noun, as in "x-ray diffraction," "4-mm-long gas cell," and "R-matrix theory." However, hyphens are deleted from word pairs when they are not used as adjectives before nouns, as in "emission by x rays," "was 4 mm in length," and "the R matrix is tested." Note also that Physical Review follows U.S. English guidelines in that hyphens are not used after prefixes or before suffixes: superresolution, quasiequilibrium, nanoprecipitates, resonancelike, clockwise.

- Please check that your figures are accurate and sized properly. Make sure all labeling is sufficiently legible. Figure quality in this proof is representative of the quality to be used in the online journal. To achieve manageable file size for online delivery, some compression and downsampling of figures may have occurred. Fine details may have become somewhat fuzzy, especially in color figures. Figures to be published in color online will appear in color on these proofs if viewed on a color monitor or printed on a color printer.
- Overall, please proofread the entire formatted article very carefully. The redlined PDF should be used as a guide to see changes that were made during copyediting. However, note that some changes to math and/or layout may not be indicated.

Ways to Respond

- Web: If you accessed this proof online, follow the instructions on the web page to submit corrections.
- Email: Send corrections to apspmteam@novatechset.com Include the accession code LC19350N in the subject line.

Practical Range Sensing with Thermal Light

Peng Kian Tan^{1,*}, Xi Jie Yeo,¹ Alvin Zhen Wei Leow¹, Lijiong Shen¹, and Christian Kurtsiefer^{1,2}

¹Centre for Quantum Technologies, 3 Science Drive 2 117543, Singapore

²Department of Physics, National University of Singapore, 2 Science Drive 3 117542, Singapore

(Received 22 March 2023; revised 7 May 2023; accepted 17 July 2023; published XX XX 2023)

Many quantum sensing suggestions rely on temporal correlations found in photon pairs generated by parametric down-conversion. In this work, we show that the temporal correlations in light with a thermal photon statistics can be equally useful for such applications. Using a subthreshold laser diode as an ultrabright source of thermal light, we demonstrate optical range finding to a distance of up to 1.8 km.

DOI: 10.1103/PhysRevApplied.0.XXXXXXX

I. INTRODUCTION

Quantum sensing uses quantum phenomena to improve the measurements of physical parameters and can be implemented in photonic, atomic, or solid-state systems [1]. Photonic quantum sensing techniques include ghost imaging and superresolution imaging [2]. Many photonic quantum sensing schemes rely on photon pairs generated in spontaneous parametric down-conversion (SPDC) [3] that can be entangled in several degrees of freedom, but most often make use of the temporal correlation between the photons [4]. Examples are range finding [5], illumination [6], and clock synchronization [7] schemes, where quantum light sources have an advantage of being stationary, and therefore carrying no obvious timing structure that may be subject to manipulation or eavesdropping. Furthermore, sensing schemes with modulated light sources may be susceptible to optical crosstalk [8], while sensing based on time-correlated light from nonmodulated sources cannot be reproduced.

In this work, we consider thermal light an alternative resource of time-correlated photons by utilizing its photon bunching property. This bunching behavior has been used to determine the length of optical fibers by time-delay measurements [9]. We demonstrate range sensing using a relatively simple thermal light source based on a subthreshold diode laser. The resulting spectral density of this source exceeds that of SPDC sources by approximately 10 orders of magnitude. As the luminosity of SPDC-based photon-pair sources is typically limited to nanowatts, such thermal light sources can substantially increase the signal in range-sensing applications where temporal correlations in nonmodulated light sources are used.

II. TIME-CORRELATED PHOTON PAIRS

Photonic sensing applications often make use of modulated light sources and seek for correlations of a returned signal with the modulation. In an attempt of moving to low light levels, one can make use of inherent temporal correlations found in photon pairs emerging from SPDC in three- or four-wave mixing processes. These processes generate pairs of photons that exhibit a strongly peaked second-order correlation function $g^{(2)}(\tau) = f(\tau/\tau_c)$, which characterizes a probability to observe a pair at a time separation τ . The function f is strongly peaked around $\tau = 0$ (with a spread on the order of a coherence time τ_c), and can be observed in specialized quantum light sources. Sensing applications based on this effect are carried out by measuring detection time differences between one photon acting as a reference, and the other one acting as a probe.

A more natural type of light is thermal light. Thermal light, such as blackbody radiation, exhibits a characteristic temporal photon bunching behavior [10], also known as the Hanbury Brown-Twiss effect [11]. This can also be described by a peaked second-order timing correlation,

$$g^{(2)}(\tau) = 1 + e^{-2|\tau|/\tau_c}, \quad (1)$$

where τ is again the timing separation of the two photodetection events, and τ_c is the coherence timescale of the temporal photon bunching where thermal photons have a tendency to be detected closer together than described by Poissonian statistical timing distribution. Similar to light generated by SPDC, the coherence timescale τ_c is inversely proportional to the spectral width $\Delta f \approx c\Delta\lambda/\lambda^2$ of the thermal light, which is given by the Fourier transform of the source power spectrum [12], such that $\Delta f = 1/\tau_c$ for single-line Gaussian spectrum. Here, λ is the central wavelength of the light, $\Delta\lambda$ the wavelength spread, and c the speed of light.

*cqtpk@nus.edu.sg

A relevant practical consideration for sensing applications is the brightness of the correlated light source. As shown in Fig. 1, SPDC light sources generate an output power below a nanowatt, or in the range of 10^4 to 10^9 photoevents per second. This limits the practicality of SPDC light-based sensing in environments with high attenuation or return loss. Another useful property in a temporal correlation measurement is the accuracy that can be practically used to infer, e.g., a time of flight for one of the photons. Timing uncertainties of semiconductor-based single-photon detectors are somewhere below a nanosecond, but more recent nanowire-based detectors may reach a few picoseconds. When identifying the temporal correlation feature in thermal light, however, it is necessary that the correlation peak is still detectable. If the coherence time of the thermal light is significantly smaller than the detector timing uncertainty, the visibility of the temporal correlation washes out and may make it impossible to identify it on top of the Poissonian background. It is therefore desirable to use thermal light sources with a spectral width below approximately equal to 1 GHz.

Thermal light with such a narrow optical bandwidth has been generated in many different ways. Early examples include single emission lines of gas discharge lamps [11]. Other methods involve transmitting laser light through random dispersion media such as suspension of microspheres [13], or a rotating ground glass plate [15]. These sources, however, have either relatively low output power due to the spatial incoherence of the randomization mechanism, or (e.g., in the case of rotating ground glass modulators) a relatively long coherence time.

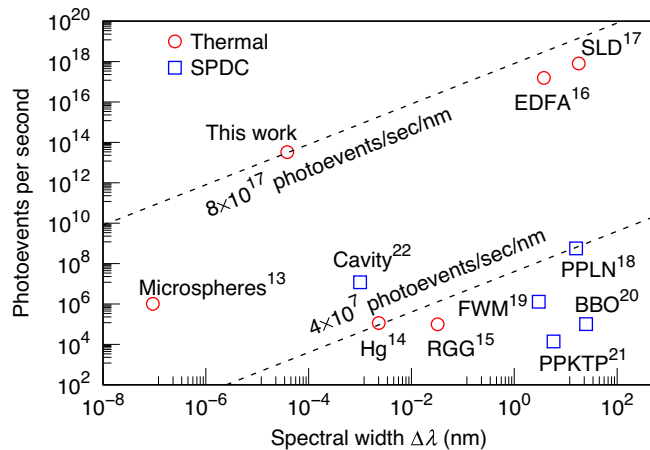


FIG. 1. Spectral densities of thermal and SPDC light sources based on the following: microspheres [13], suspension of microspheres; Hg [11,14], mercury discharge lamp; RGG [9,15], rotating ground glass; EDFA [16], erbium-doped fiber amplifier; SLD [17], superluminescent diode; PPLN [18], periodically poled lithium niobate; FWM [19], four-wave mixing; BBO [20], beta-barium borate; PPKTP [21], periodically poled potassium titanyl phosphate; cavity [22], enhancement by microring resonator.

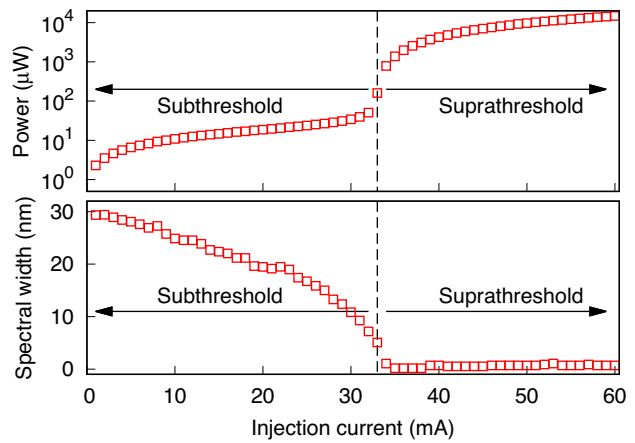


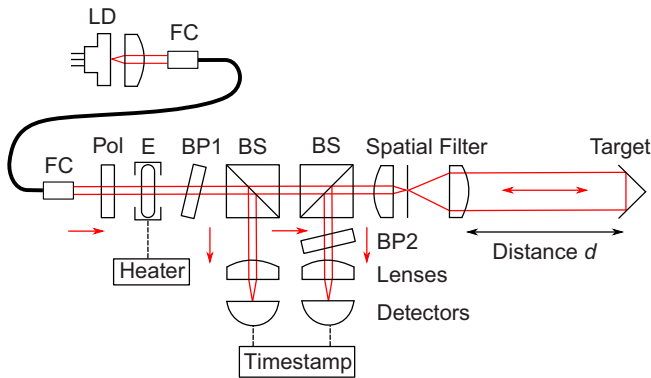
FIG. 2. Output power and spectral width $\Delta\lambda$ of a laser diode as a function of its injection current to determine the lasing threshold.

Here, we use a laser diode operating below the lasing threshold [23,24] to generate thermal light [25,26]. This amplified spontaneous emission process generates significantly higher output power in the range of $10 \mu\text{W}$ to 100 mW . Light sources of a similar category include superluminescent diodes, and erbium-doped fiber amplifiers. These examples tend to have spectral densities above milliwatts per nanometer.

The diode laser we use (nominal lasing wavelength $\lambda = 518 \text{ nm}$, single spatial mode output) shows a lasing threshold current around 33 mA (see Fig. 2), where the output power exhibits a sharp increase of 3 orders of magnitude, and the spectrum narrows to a single emission line, limited by the grating spectrometer to about 0.3 nm . We operate the diode laser at a subthreshold current of 32.9 mA , where it exhibits the photon bunching behavior that is characteristic of thermal light. The light is then coupled into a single spatial mode optical fiber. We observe an optical power of $12.5 \mu\text{W}$, corresponding to a photon rate $R \approx 3.3 \times 10^{13} \text{ s}^{-1}$, within a spectral window of $\Delta f = 43 \text{ MHz}$. This results in a thermal light source of extremely high spectral brightness of about 8×10^{17} photoevents per second and nanometer.

III. RANGE-SENSING SETUP

The stationary thermal light generated from a subthreshold laser diode is implemented into an optical ranging setup based on time-of-flight measurements, commonly known as light distance and ranging (lidar) (see Fig. 3). While conventional lidar introduces timing modulation [8,27] into the intensity, amplitude, or phase of the light source, to provide timing correlations, this work relies on photon bunching of thermal light to provide the timing correlations. We do record the photodetection events with



F3:1 FIG. 3. Experimental setup using thermal light for ranging
F3:2 measurements. LD, laser diode; FC, fiber coupler; Pol, polarizer;
F3:3 E, etalon; BP1, BP2, bandpass filters; BS, beam splitter.

142 a high timing resolution to obtain the temporal photon
143 bunching signature $g^{(2)}(\tau)$ similar to Ref. [28].

144 To ensure that we select only a single chip mode of thermal
145 light from the subthreshold laser diode, a combination
146 of a polarization filter, a bandpass filter (BP1 in Fig. 3)
147 and a temperature-tuned etalon is used. The etalon is based
148 on a fused silica (Suprasil311) substrate and has a tuning
149 parameter of 4 GHz/K for its resonances. Optical coatings
150 with a reflectivity of 97% on both sides result in a finesse
151 of 103. The plano-parallel substrate has a thickness of 0.5
152 mm, resulting in a free spectral range of about 205 GHz,
153 and spectral transmission windows of 2 GHz FWHM [29].
154 This allows effective suppression of adjacent laser-diode
155 chip modes, which are separated by about 50 GHz from
156 the mode used. The bandpass interference filter BP1 has a
157 2-nm-wide passband centered at $\lambda = 518$ nm to suppress
158 source light beyond the free spectral range of the etalon.

159 An asymmetric beam splitter directs 92% of the filtered
160 thermal light into the probe beam and retains 4% as a local
161 reference beam sent to a first single-photon detector.

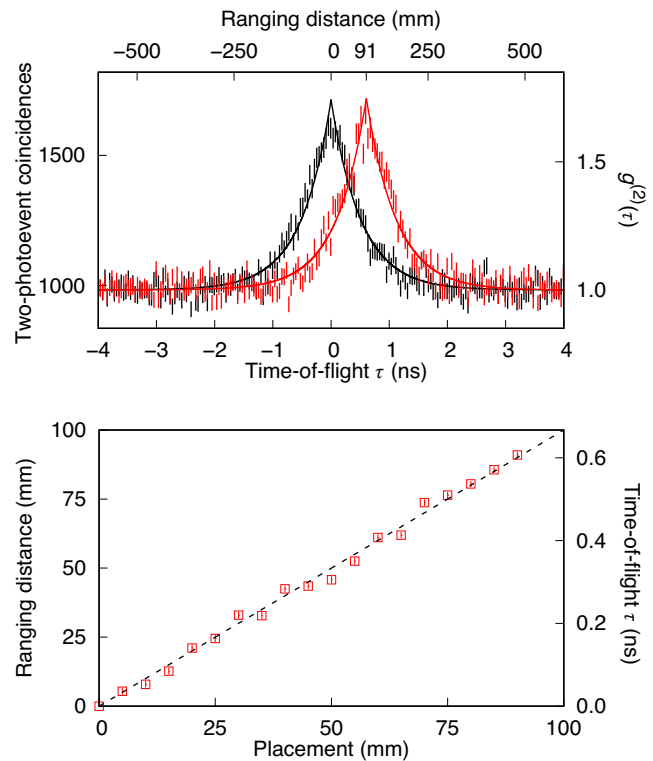
162 The spectrally filtered thermal light beam passes through
163 a 50:50 beam splitter and a telescope formed by a lens pair
164 ($f = 50$ mm, $f = 300$ mm) around a spatial filter, and is
165 expanded to a diameter of about 50 mm. The probe beam
166 returns from the target reflector through the same telescope
167 and beam splitter onto the probe photodetector. The spatial
168 filter cleans up the returning probe beam and reduces ambient
169 light contribution from reaching the detectors, and the
170 use of a second beam splitter ensures that no breakdown
171 flash light from the target detector can reach the reference
172 photodetector. A second bandpass filter BP2 is used
173 to suppress ambient light reaching the probe detector.

174 The $g^{(2)}(\tau)$ photon bunching peak is shifted by a time
175 $\tau_0 = 2d/c$ in its timing position, corresponding to the
176 optical path-length difference between probe and reference
177 beam, thus allowing the distance d of a target retroreflector
178 to be inferred from the peak position of $g^{(2)}(\tau)$.

Both single-photon detectors are actively quenched silicon avalanche photodiodes with a quantum efficiency about 50% at 550 nm, and a timing jitter around 40 ps. The detected photoevents are timestamped by an oscilloscope with (sampling rate 40 GSPS), and time differences were histogrammed into 40-ps-wide time bins for short distances d , or recorded with an FPGA-based timestamp device with a resolution of 2 ns and sorted into 2-ns-wide time bins numerically for long distances d .

IV. RANGE-SENSING DEMONSTRATIONS

Figure 4 shows two representative time-difference histograms together with a fitted second-order timing correlation function $g^{(2)}(\tau)$ according to Eq. (1). These allow determination of the positions τ_0 of their respective bunching peaks and the corresponding ranging distances d from the round-trip time of the probe beam for a set of target placement positions (Fig. 4, bottom trace). The resulting ranges are in good agreement with their corresponding target placement positions, and compatible with a constraint in the detector timing jitter (about 40 ps FWHM).



F4:1 FIG. 4. Top: photon bunching $g^{(2)}(\tau)$ measurements with the
F4:2 target reflector placed at 0 (black) and 90 mm (red). The solid
F4:3 line represents a fit to Eq. (1) resulting in $\tau_c = 1.03 \pm 0.03$ ns,
F4:4 a peak displacement of $\tau_0 = 0.606 \pm 0.008$ ns corresponding to
F4:5 a ranging distance of $d = 91.0 \pm 1.2$ mm, with a reduced χ^2 of
F4:6 1.19. Bottom: ranging distances extracted from fits to the bunching
F4:7 signatures as a function of the placement positions to test for
F4:8 distance resolution.

To demonstrate the robustness of the ranging setup, we conducted two outdoor field measurements. Figure 5 shows two long-range time-of-flight measurements together with a reference zero position (black trace), resulting in the ranging distances of 965.29 ± 0.02 m (blue) and $1,851.48 \pm 0.02$ m (red) fitted to Eq. (1) with reduced χ^2 of 1.09 and 1.05, respectively, under the assumption of a unit refractive index of air. The increased uncertainty compared to the short-range measurements shown in Fig. 4 are due to the more coarse histogramming for this experiment.

For the long-distance measurements, the etalon temperature tuning and stability was improved relative to the measurements in Fig. 4, increasing the coherence timescale $\tau_c = 23.2 \pm 0.4$ ns (red), corresponding to a spectral linewidth $\Delta f = 43$ MHz.

The temporal photon bunching peak (red) is slightly reduced to $g^{(2)}(\tau = 0) = 1.591 \pm 0.009$ (red) due to an increase of the bin width from 40 ps to 2 ns for the time differences, and by noise contribution from ambient light to the probe detector.

The detection rate at the probe detector was fluctuating around 10^5 s $^{-1}$. With the emission rate of

$R \approx 3.3 \times 10^{13}$ s $^{-1}$, this corresponds to a return loss of 80 to 90 dB in that experiment.

V. SIGNAL-TO-NOISE CONSIDERATIONS

The very high spectral density of our light source helps to increase the signal-to-noise ratio [30,31] of a bunching peak detection significantly. When photodetectors are fast enough to resolve the temporal coherence τ_c of the photon bunching signature, the SNR of the second-order correlation function $g^{(2)}(\tau)$ will be dominated by shot noise of the photodetection events, and can be described by

$$\text{SNR} = r \times V^2 \sqrt{\tau_c \cdot \Delta T}, \quad (2)$$

with the photoevent rate r , the interferometric visibility $V = \sqrt{g^{(2)}(0) - 1}$, the coherence time τ_c , and the integration time ΔT .

With a photon bunching peak value $V^2 = 0.6$ and a coherence timescale $\tau_c = 23$ ns, which corresponds to the measured values in Fig. 5, an upper bound for the signal-to-noise ratio of around 30 can already be achieved after an integration time $\Delta T = 1$ ms at a photodetection rate of $r = 10^7$ s $^{-1}$ given by typical avalanche photodetector saturation. This high tolerance to attenuation provides the thermal light source an advantage over SPDC light sources in practical sensing use cases where significant losses can be expected.

VI. SUMMARY

This work explored the use of thermal light for applications where measurements (like range finding) are based on detecting correlations in time. Subthreshold lasers with their intrinsic temporal correlations thus provide a powerful alternative to light sources based on spontaneous parametric down-conversion in quantum sensing applications, and may offer superior signal-to-noise ratios at a much reduced system complexity.

With such light sources, a technique originally used for estimating the size of stars half a century ago can boost a wide range of practical quantum sensing applications that mostly rely on temporal correlations.

ACKNOWLEDGMENTS

This research is supported by the Quantum Engineering Programme through Grants No. QEP-P1 and No. NRF2021-QEP2-03-P02, the National Research Foundation, Prime Minister's Office, Singapore.

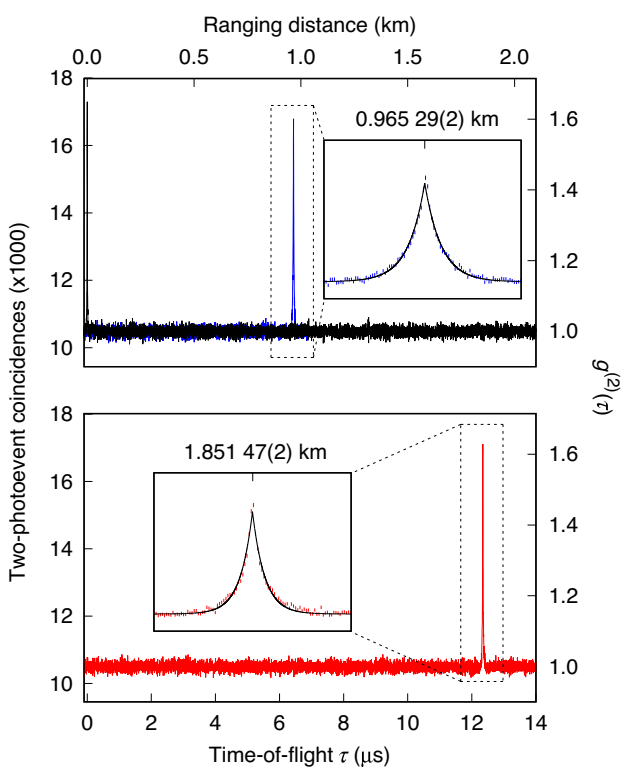


FIG. 5. Optical ranging measurements to the reference zero distance position with the retroreflector placed at the telescope aperture (top, black trace), and the signal obtained with a retroreflector about 1-km away (top, blue trace). The bottom trace shows the bunching signature with the target retroreflector located about 1.8 km away from the reference detector.

- [1] S. Pirandola, B. R. Bardhan, T. Gehring, C. Weedbrook, and S. Lloyd, Advances in photonic quantum sensing, *Nat. Photon.* **12**, 724 (2018).

- [2] P.-A. Moreau, E. Toninelli, T. Gregory, and M. J. Padgett, Imaging with quantum states of light, *Nat. Rev. Phys.* **1**, 367 (2019).
- [3] R. Ghosh and L. Mandel, Observation of Nonclassical Effects in the Interference of Two Photons, *Phys. Rev. Lett.* **59**, 1903 (1987).
- [4] A. S. Clark, M. Chekhova, J. C. F. Matthews, J. G. Rarity, and R. F. Oulton, Special topic: Quantum sensing with correlated light sources, *Appl. Phys. Lett.* **118**, 060401 (2021).
- [5] S. Frick, A. McMillan, and J. Rarity, Quantum range finding, *Opt. Express* **28**, 37118 (2020).
- [6] E. D. Lopaeva, I. R. Berchera, I. P. Degiovanni, S. Olivares, G. Brida, and M. Genovese, Experimental Realization of Quantum Illumination, *Phys. Rev. Lett.* **110**, 153603 (2013).
- [7] C. Ho, A. Lamas-Linares, and C. Kurtsiefer, Clock synchronization by remote detection of correlated photon pairs, *New J. Phys.* **11**, 045011 (2009).
- [8] S. Royo and M. Ballesta-Garcia, An overview of lidar imaging systems for autonomous vehicles, *Appl. Sci.* **9**, 4093 (2019).
- [9] J. Zhu, X. Chen, P. Huang, and G. Zeng, Thermal-light-based ranging using second-order coherence, *Appl. Opt.* **51**, 4885 (2012).
- [10] R. Glauber, The quantum theory of optical coherence, *Phys. Rev.* **130**, 2529 (1963).
- [11] R. Hanbury-Brown and R. Q. Twiss, Correlation between photons in two coherent beams of light, *Nature* **177**, 27 (1956).
- [12] M. Fox, *Quantum Optics: An Introduction* (Oxford University Press, UK, 2006).
- [13] D. Dravins, T. Lagadec, and P. D. Nunez, Optical aperture synthesis with electronically connected telescopes, *Nat. Commun.* **6**, 6852 (2015).
- [14] P. K. Tan, A. H. Chan, and C. Kurtsiefer, Optical intensity interferometry through atmospheric turbulence, *MNRAS* **457**, 4291 (2016).
- [15] F. T. Arecchi, Measurement of the Statistical Distribution of Gaussian and Laser Sources, *Phys. Rev. Lett.* **15**, 912 (1965).
- [16] P. Janassek, A. Herdt, S. Blumenstein, and W. Elsaber, Ghost spectroscopy with classical correlated amplified spontaneous emission photons emitted by an erbium-doped fiber amplifier, *Appl. Sci.* **8**, 1896 (2018).
- [17] A. T. M. A. Rahman and P. F. Barker, Optical levitation using broadband light, *Optica* **7**, 906 (2020).
- [18] Z. Zhang, S. Mouradian, F. N. C. Wong, and J. Shapiro, Entanglement Enhanced Sensing in a Lossy and Noisy Environment, *Phys. Rev. Lett.* **114**, 110506 (2015).
- [19] D. G. England, B. Balaji, and B. J. Sussman, Quantum-enhanced standoff detection using correlated photon pairs, *Phys. Rev. A* **99**, (2019).
- [20] A. Lohrmann, A. Villar, A. Stolk, and A. Ling, High fidelity yield stop collection for polarization-entangled photon pair sources, *Appl. Phys. Lett.* **113**, 171109 (2018).
- [21] Y.-C. Jeong, K.-H. Hong, and Y.-H. Kim, Bright source of polarization-entangled photons using a ppktp pumped by a broadband multi-mode diode laser, *Opt. Express* **24**, 1165 (2016).
- [22] T. J. Steiner, J. E. Castro, L. Chang, Q. Dang, W. Xie, J. Norman, J. E. Bowers, and G. Moody, Ultrabright Entangled Photon Pair Generation from an AlGaAs on Insulator Microring Resonator, *Phys. Rev. X* **2**, 010337 (2021).
- [23] M. G. A. Bernard and G. Duraffourg, Laser conditions in semiconductors, *Phys. Status Solidi B* **1**, 699 (1961).
- [24] G. Lasher and F. Stern, Spontaneous and stimulated recombination radiation in semiconductors, *Phys. Rev.* **133**, (1964).
- [25] W. Shockley and J. W. T. Read, Statistics of the recombinations of holes and electrons, *Phys. Rev.* **87**, (1952).
- [26] D. T. Cassidy, Spontaneous-emission factor of semiconductor diode lasers, *JOSA B* **8**, 747 (1991).
- [27] G. Beheim and K. Fritsch, Range finding using frequency-modulated laser diode, *Appl. Opt.* **25**, 1439 (1986).
- [28] P. K. Tan and C. Kurtsiefer, Temporal intensity interferometry for characterization of very narrow spectral lines, *MNRAS* **469**, 1617 (2017).
- [29] P. K. Tan, G. H. Yeo, H. S. Poh, A. H. Chan, and C. Kurtsiefer, Measuring temporal photon bunching in blackbody radiation, *ApJL* **789**, L10 (2014).
- [30] R. Hanbury-Brown, *The Intensity Interferometer: Its Application To Astronomy* (Taylor & Francis; Halsted Press, London; New York, 1974), 184
- [31] C. Foellmi, On the intensity interferometry and the second-order correlation function $g^{(2)}$ in astrophysics, *A&A* **507**, 1719 (2009).